

**Advanced Methods for Predicting 3D
Unsteady Flows Around Wind Turbine
Blades**

**to
Continuum-Dynamics, Inc.**

Final Report

**in support of
DOE Phase I STTR
October 27, 2010 – March 18, 2011**

Submitted by:

**Marilyn J. Smith
School of Aerospace Engineering
Georgia Institute of Technology
Atlanta, GA 30332-0150**

March 18, 2011

Table of Contents

Summary	3
Introduction	Error! Bookmark not defined.
Review of Wind Turbine Aerodynamics and Fluid Structure Interactions	Error! Bookmark not defined.
Wind Turbine Analysis Methods: Overview	Error! Bookmark not defined.
Wind Turbine Analysis Methods: Blade Aerodynamics	Error! Bookmark not defined.
Wind Turbine Analysis Methods: Wake Prediction	Error! Bookmark not defined.
Overview of VorTran-M	Error! Bookmark not defined.
Formulation	Error! Bookmark not defined.
Demonstration and Validation of VorTran-M: RSA3D/VorTran-M	Error! Bookmark not defined.
Anticipated Public Benefits	Error! Bookmark not defined.
Degree to which Phase I has Demonstrated Technical Feasibility	Error! Bookmark not defined.
Executive Summary	Error! Bookmark not defined.
Review of Phase I	Error! Bookmark not defined.
FUN3D/VorTran-M Partial Parallelization	9
Interface with Actuating Blade Approach	9
Validation	Error! Bookmark not defined.
Steady Fixed Wing	11
Unsteady Fixed Wing	11
Circular Cylinder in a Cross-Flow	12
Two-Bladed Hovering Rotor	16
Phase II Technical Objectives	Error! Bookmark not defined.
Phase II Work Plan	Error! Bookmark not defined.
Task 1: Kickoff Briefing and Refinement of Work Plan (Lead: G.R. Whitehouse; Support: A.H. Boschitsch and M.J. Smith; Duration: 1 month)	Error! Bookmark not defined.
Task 2: Interface Upgrades	Error! Bookmark not defined.
2.1: Acoustics Interface Development (Lead: M.J. Smith; Support: G.R. Whitehouse; Duration: 1 month)	Error! Bookmark not defined.
2.2: Dynamics Interface Development (Lead: M.J. Smith; Support: G.R. Whitehouse; Duration: 1 month)	Error! Bookmark not defined.
2.3: Continued Evaluation of FUN3D Boundary Conditions (Lead: M.J. Smith; Support: G.R. Whitehouse and A.H. Boschitsch; Duration: 1 month)	Error! Bookmark not defined.
2.4: Atmospheric Boundary Layer Model Plug-in Development (Lead: G.R. Whitehouse; Support: A.H. Boschitsch and M.J. Smith; Duration: 1 month)	Error! Bookmark not defined.
Task 3: Parallelize VorTran-M (Lead: G.R. Whitehouse; Support: A.H. Boschitsch and M.J. Smith; Duration: 1 month)	Error! Bookmark not defined.
Task 3.1: Decouple the Grid Structure from the Velocity Calculation (Lead: G.R. Whitehouse; Support: A.H. Boschitsch; Duration: 1 month)	Error! Bookmark not defined.
Task 3.2: Development of hybrid velocity calculation	Error! Bookmark not defined.
Task 3.3: Parallel algorithm development	Error! Bookmark not defined.
Task 4: Sample Calculations and Validation (Lead: G.R. Whitehouse; Support: M.J. Smith, A.H. Boschitsch; Duration: 6 months)	Error! Bookmark not defined.
Task 4: Documentation and Reporting (Lead: G.R. Whitehouse, Support: M.J. Smith, A.H. Boschitsch; Duration: 2 months)	Error! Bookmark not defined.
Phase II Performance Schedule	Error! Bookmark not defined.
Additional Related Research and Bibliography	Error! Bookmark not defined.
Related R&D	Error! Bookmark not defined.
References Cited	18
Principal Investigator and other Key Personnel	Error! Bookmark not defined.
Facilities/Equipment	Error! Bookmark not defined.
Consultants and Subcontractors	Error! Bookmark not defined.
Phase II Funding Commitment	Error! Bookmark not defined.
Phase III Follow-On Funding Commitment	Error! Bookmark not defined.

List of Figures

Figure 1: Aerial photograph of offshore wind farm wake interaction (Horns Rev, Denmark)	6
Figure 2: The wind farm flow environment is extremely complicated and current approaches neglect key physics	6
Figure 3: Various wind turbine designs: (a) cup-anemometer; (b) stacked Savonius rotor; (c) modern HAWT; (d) Darrieus VAWT; (e) H-rotor VAWT	Error! Bookmark not defined.
Figure 4: Wake visualization behind a one-bladed downstream facing HAWT [18]...	Error! Bookmark not defined.
Figure 5: CFD predictions of rotor wake vorticity. (a) Two bladed rotor in hover, slice at $\Psi=80^\circ$ [35] (b) Two bladed rotor in forward flight [36] (c) UH-60A rotor in hover [34] (d) UH-60 Rotor in Forward Flight [11].....	Error! Bookmark not defined.
Figure 6: Wake Visualization of a Two Bladed Hovering Rotor [52].....	Error! Bookmark not defined.
Figure 7: VTM wind turbine predictions. HAWT wake interaction [53] (top left), VAWT simulation [54] (top right) and comparison with RANS HAWT wake prediction [55] (bottom)	Error! Bookmark not defined.
Figure 8: Iso-surface of vorticity magnitude showing the effects of flux-limiting on wake structure. MIN-type flux limiter (left) and SUPER-type flux limiter (right) [51]	Error! Bookmark not defined.
Figure 9: Schematic of the coupling between VorTran-M and PV CFD	Error! Bookmark not defined.
Figure 10: Wake geometry expressed as vorticity iso-surface for the rectangular wing positioned normal to the flow (left) and force time history (right).....	Error! Bookmark not defined.
Figure 11: Vorticity iso-surface in the rotor wake and pressure contours on the RSA3D boundary for an untrimmed rotor in slow speed ascent (top left); slow speed forward flight (top right) and high speed forward flight (bottom).....	Error! Bookmark not defined.
Figure 12: Predictions of wake vorticity, plotted at the same level of vorticity magnitude, for a 1-bladed rotor in forward flight after 2550 time steps. OVERFLOW near body grids bounded in red and VorTran-M grid in blue	Error! Bookmark not defined.
Figure 13: Predicted vorticity magnitude for a single-bladed rotor in forward flight on a plane perpendicular to the direction of flight, a) 23.2, b) 31.7, c) 33 and d) 40 chord lengths and downstream of the hub. Δ_{OVERFLOW} (outlined at left) $\approx 0.22c$, Δ_{OVERFLOW} (outlined region at left) $\approx 0.43c$ and $\Delta_{\text{VorTran-M}} \approx 0.43c$.	Error! Bookmark not defined.
Figure 14: Close-up of OVERFLOW (upper) and OVERFLOW/VorTran-M (lower) predictions of the near-body wake and velocity vectors on a slice through the rotor from [62]	Error! Bookmark not defined.
Figure 15: Comparison of measured and predicted spanwise loading ($C_{T \text{ Experiment}} = 0.0046$, $C_{T \text{ OVERFLOW}} = 0.00432$, $C_{T \text{ OVERFLOW/VorTran-M}} = 0.00458$) from [62] (left). Comparison of measured and predicted tip vortex trajectory (right)	Error! Bookmark not defined.
Figure 16: Hover Performance for a 1:5.73 scale Sikorsky UH-60A main rotor, compared to measurements from [64]. $M_{\text{tip}}=0.64$	Error! Bookmark not defined.
Figure 17: Predictions of a NACA0012 wing at 90 degrees angle of attack run in, (a) OVERFLOW 2.0 Spalart-Allmaras RANS; (b) OVERFLOW 2.0 Advanced RANS-LES; (c) FUN3D Spalart-Allmaras RANS (d) FUN3D/VorTran-M.....	7
Figure 18: Sample scalability. Open symbols: computational speed-up; solid symbols: computational efficiency.	Error! Bookmark not defined.
Figure 19: Actuating blades schematic; sources are located at the planform grid intersections and rotate with the blades (left). Incompressible wake simulation of an NREL rotor in 15m/s wind using an actuating blade with FUN3D (right)	10
Figure 20: Simple four-bladed rotor in hover	10
Figure 21: Iso-surfaces of vorticity magnitude for pitching NACA0012 wing predicted with FUN3D/VorTran-M ..	12
Figure 22: Comparisons of vorticity magnitude for an oscillating wing simulated with FUN3D and FUN3D/VorTran-M.....	13
Figure 23: Comparisons of lift (left) and (right) moment coefficients for an oscillating wing.....	13
Figure 24: FUN3D and FUN3D/VorTran-M predictions of the drag on a circular cylinder (left) and the FUN3D/VorTran-M predicted wake structure (right).....	14
Figure 25: Schematic of FUN3D/VorTran-M grid arrangement for the two bladed rotor in hover.....	17
Figure 26: Snapshots of the hovering rotor wake predicted by FUN3D/VorTran-M.....	17
Figure 27: Permeable surfaces for acoustics calculations. Rotating surface that encloses a single blade (left) and non-rotating surface enclosing the entire rotor (right).....	Error! Bookmark not defined.
Figure 28: Flat plate configuration embedded in a near-body FUN3D tetrahedral mesh (left) and vorticity shed from the flat plat in a free stream velocity of 25 m/s (right)	Error! Bookmark not defined.

Figure 29: Recirculation effects for an oscillating flat plate. Original Riemann boundary condition (left) and modified Riemann boundary condition (right) **Error! Bookmark not defined.**

Figure 30: Schematic of cell creation and destruction (left) and nested grid structure in VorTran-M..... **Error! Bookmark not defined.**

Figure 31: VorTran-M adaptive grid for a rotor in climbing flight with $O(10^5)$ active cells (left). Note that cells are only required in vorticity containing regions. Conventional Cartesian adaptive grid for a hovering rotor with $O(10^8)$ active cells from [75] (right). Note that for conventional CFD solvers, cells are required everywhere. **Error! Bookmark not defined.**

Figure 32: Schematic diagram of grid structure for Poisson solution **Error! Bookmark not defined.**

Figure 33: Diverse systems modeled with CDI FMM methods – vortex breakdown and crow instability in multipair systems (top – 12,000 vortex elements); electrical potential of the Carboxypeptidase A molecule, including dielectric screening effects (bottom - ~480 atoms and a molecule composed of ~55,000 elements) **Error! Bookmark not defined.**

Figure 34: Aeronautical systems studied with fast vortex/fast panel methods enabled by hierarchical FMM techniques (left to right); V-22 tiltrotor; EH-101 helicopter; Space Shuttle; F-15**Error! Bookmark not defined.**

Figure 35: Schematic diagram of boundary conditions for Poisson solution **Error! Bookmark not defined.**

Figure 36: Partitioning of sample VorTran-M solution domain for a rotor at startup ..**Error! Bookmark not defined.**

Figure 37: Speed-up of the parallel FMM VorTran-M module calculating the roll-up of a vortex sheet (left) and Parallel Poisson solver VorTran-M speed-up (with respect to 4 processors) on a problem with 7.1 Million points per processor(right)..... **Error! Bookmark not defined.**

Figure 38: Computational cost of the parallel FMM and Poisson solutions for the same 3D vortex ring evolution problem **Error! Bookmark not defined.**

Figure 39: Unstructured grid for the NREL Phase VI HAWT configuration. 2.6 million nodes per blade, 7.2 million nodes total.18

Figure 40: Comparison of the predicted vorticity magnitude for FUN3D hybrid RANS-LES (left) and RANS (right) wakes for a circular cylinder.....8

Figure 41: Hybrid RANS-LES prediction of flow over a DU97W300 flatback airfoil section (left); predictions of the flow around a full HAWT configuration (center and right).....8

Summary

Wind power has an important role to play in satisfying the power requirements of the United States. Since wind power is a clean renewable source of energy, it also serves an important role in reducing our dependence on fossil fuels, in particular foreign oil supplies, for power generation as well as reducing greenhouse gas and carbon emissions. Unfortunately, significant long term maintenance costs, recently highlighted by a series of blade failures [1-3], are related to fatigue induced by unsteady loading and wake interactions related to installation layout (i.e. large scale land-based and offshore wind farms) and off-design wind conditions. While much research has been performed to understand the aerodynamic loading on isolated wind turbines, little has been done to understand and mitigate the fluid-structure-interactions (FSI) that contribute to structural fatigue and the characteristic noise associated with wind turbine blades passing the support structure. FSI and noise are further complicated when innovative wind turbine concepts feature more blades and vertical axis configurations, both of which promote more frequent and potentially noisy interactions. In fact, fatigue induced by FSI was one of the major factors that led to the cancellation of all large-scale vertical axis projects in the U.S. and Canada. In this vein, the proposed research program will develop an advanced methodology for accurately capturing blade loading, long period wakes and unsteady effects influencing wind turbine fatigue and noise-inducing FSI, in particular multiple wind turbine interactions (see, for example, Figure 1), so that modifications can be made to address these issues early in the design process of wind turbines and wind farms. In addition, as advanced inflow models of the atmospheric boundary layer (ABL), under development through other funding mechanisms, become available, they can be interfaced directly with this methodology. Thus a successful effort will pave the way for the development of quieter, more efficient wind turbines with enhanced longevity and reduced maintenance costs.

The Phase I effort built upon the mutually supporting experience of the team of Continuum Dynamics, Inc (CDI) and Georgia Institute of Technology (GIT) by leveraging prior and ongoing research into wind turbine/rotorcraft aeromechanics and wake prediction (specifically numerical diffusion, grid generation, turbulence modeling and rotorcraft and horizontal axis wind turbine (HAWT) noise prediction and reduction) to directly address the issue of wind turbine FSI. To address the inherent numerical diffusion of vorticity in RANS methods [4], this effort applied CDI's VorTran-M modular CFD solver to long age wakes, and captured near-body wakes via hybrid RANS coupling. To demonstrate the concept, and to develop the most efficient coupling methodology, this effort has integrated and demonstrated the concept using the NASA FUN3D massively parallel unstructured grid RANS analysis [5]. This methodology is capable of resolving both the incompressible and compressible RANS equations to handle the gamut of wind turbine conceptual designs, and it has been extended in prior and ongoing work by the project team members to include overset methods for rotating frames [6, 7], support for hybrid RANS-LES turbulence modeling [8] and FSI using both beam and full-surface computational structural dynamics (CSD) modeling via DYMORE and RCAS [9, 10]. This approach provides critical flexibility to the end user by providing a coupled FUN3D/VorTran-M tool (interfaced with a structural dynamics code if desired) that can be obtained for design and analysis, or a toolkit with which to rapidly couple VorTran-M with the researcher's own RANS, or even LES, methodology in which they have investigated significant internal resources developing.



Figure 1: Aerial photograph of offshore wind farm wake interaction (Horns Rev, Denmark)

Prior Work

Wind turbine technology has progressed at an impressive rate over the past decades, due in part to financial support from government incentives and in part to engineering initiatives by the U.S. DOE and others. Despite the significant large-scale operational experience accumulated over this time period, wind power systems are still undergoing considerable maturation, and improvements are still required in their design if they are to compete with non-renewable energy sources. In particular, relatively little is known about fatigue and noise inducing FSIs related to off-design wind conditions and installation effects (i.e. wind farm interactions), as illustrated in Figure 2.

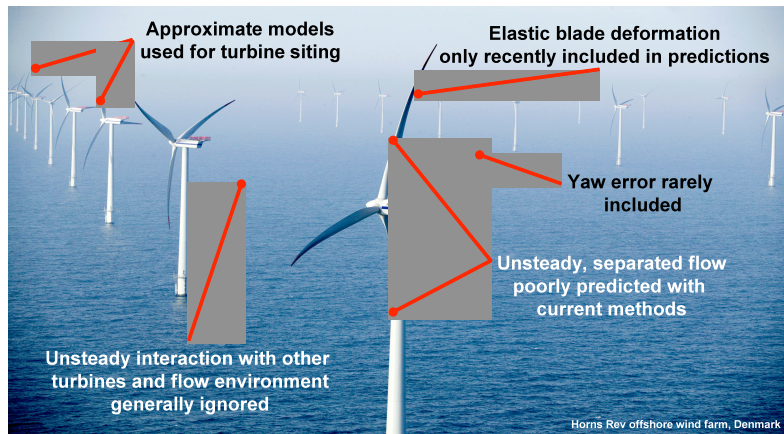


Figure 2: The wind farm flow environment is extremely complicated and current approaches neglect key physics. {Modifications to photo courtesy of CDI.}

FUN3D is a parallel, unstructured grid computational fluid dynamics (CFD) solver that has been and continues to be developed at NASA Langley Research Center (LaRC). This solver includes many state of the art capabilities, such as adjoint-based error estimation, mesh adaptation for static configurations, and design optimization [5]. The FUN3D methodology was originally developed for fixed-wing applications; however, recently it has been extended to evaluate rotary-wing applications by Smith and co-workers at GIT [6, 12], as well as other members of the FUN3D development team [13]. Moreover, this CFD tool has been integrated with the DYMORE and RCAS rotorcraft computational structural dynamics (CSD) solvers to accurately account for blade motion and structural deformation [12] at GIT, as well as integration with CAMRAD II at NASA [13] using beam model assumptions for the blades. Given these recent advances, in addition to the desire to develop a computational tool suitable for

routine design and analysis without requiring extensive mesh generation and repair tasks that require significant human interaction, it is currently envisioned that FUN3D can function as the host solver for plethora of multidisciplinary analyses.

The flow field for a wing at 90° angle of attack is highly unsteady and dominated by vorticity shed and trailed from the edges of the wing. To provide a benchmark, FUN3D computations for a semi-infinite wing are shown in Figure 3a and b, where the predicted vorticity shed from the wing with a traditional turbulence model on a typical “industry-size” grid shows separation at the upper and lower surfaces, with some wake shedding that is rapidly dissipated. The use of a more refined grid and an advanced hybrid RANS-LES turbulence model improves the simulation, where much more distinct vortices can be observed being shed from the surface, but these are dissipated very rapidly in the wake as well.

The flow field predicted on the FUN3D grid (with Spalart-Allmaras turbulence model) is similar to the OVERFLOW Spalart-Allmaras results. Likewise, the FUN3D/VorTran-M prediction shows significant similarities to the OVERFLOW RANS-LES method on a much larger and more refined CFD grid. The predicted location and orientation of the vortex sheet from the wing are in approximately the same for OVERFLOW RANS-LES and FUN3D/VorTran-M; however, the VorTran-M prediction is far less dissipative. The integrated drag force on the wing predicted by the coupled FUN3D/VorTran-M simulation are very similar to the predictions of the OVERFLOW hybrid RANS-LES simulation, and, with refinement, exhibit the expected asymptote to the theoretical flat plate value of 2.0.

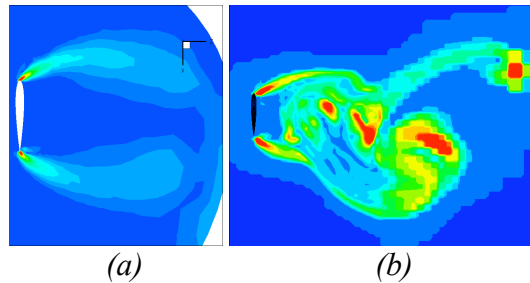


Figure 3: Predictions of a NACA0012 wing at 90 degrees angle of attack run in, (a) FUN3D Spalart-Allmaras RANS (b) FUN3D/VorTran-M

Under a grant from the National Science Foundation, Georgia Tech has extended the application of FUN3D to HAWT configurations. This work is exploring the ability of advanced turbulence modeling, CFD/CSD coupling for blade FSI, and locally adapting grids from rotorcraft to model the full HAWT configuration (blade, nacelle and tower). Further, these methods are being extended to handle the incompressible high Reynolds number flows of large HAWT systems. This effort, entering its final year of a three-year effort, has resulted in several publications discussing various aspects of the noise and interactional aerodynamics of large HAWTs [27, 28]. The advanced hybrid RANS-LES (HRLES) turbulence models have been extended to unstructured methods and have been successfully verified on a canonical LES test case, a cylinder at $M=0.2$, $Re=3900$, which is similar to HAWT towers. Figure 4 shows that HRLES captures the physics associated with the vortex shedding more accurately than a $k-\omega$ -SST RANS approach on an identical grid; the RANS solution smoothes out the vortex shedding process, whereas the vortex wake of the HRLES is much more realistic. The instantaneous pressure coefficient on the cylinder indicates that the magnitude of the HRLES simulation is within 3% of the experimental data, while the RANS model is approximately 18% different. The

separation point is also captured within the experimental error using the hybrid RANS-LES model, while the RANS solution is more than 10% too far aft.

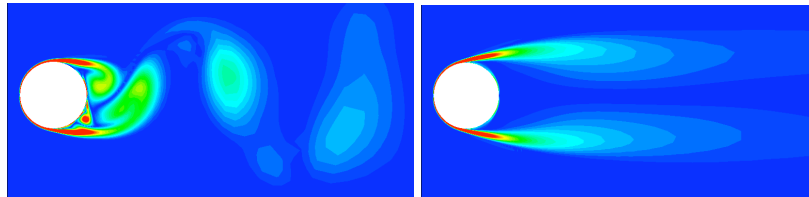


Figure 4: Comparison of the predicted vorticity magnitude for FUN3D hybrid RANS-LES (left) and RANS (right) wakes for a circular cylinder

A collaborative effort with Sandia Labs compared results with different turbulence simulation methods with experimental data for the DU97W300 flatback wind turbine airfoil [95], and indicated the need for a turbulence simulation methodology that is fully three-dimensional to capture the full wake of the airfoil (Figure 5 left). The results in this paper have been extended, and recent results show a dramatic improvement of the ability of the hybrid method to capture the Strouhal number (200% improvement).

Recent efforts have focused on full tower simulations, as illustrated in Figure 5, which illustrate the capability of the FUN3D solver to capture the near-field wake complexity of the Phase VI HAWT rotor/nacelle/tower combination. This simulation uses three overset grids: tower/nacelle in the inertial frame and two blade grids that rotate about the nacelle, however, beyond the 2-3 revolution mark, the wake simulation begins to diffuse significantly.

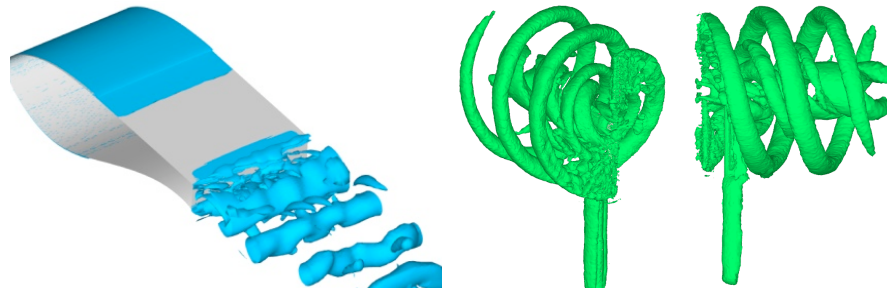


Figure 5: Hybrid RANS-LES prediction of flow over a DU97W300 flatback airfoil section (left); predictions of the flow around a full HAWT configuration (center and right)

The wake structure is critically important to the calculation of accurate aeroelastic phenomena, including quasi-steady performance characteristics. CFD methods suffer from the inability to accurately model the wake over long wake ages without a significant increase in grid resolution, and by extension computational resources [15], and so alternatives are sought. A different formulation of the Navier-Stokes equations, namely the Vorticity Transport Method (VTM), has been successfully applied to wind turbine wakes [14]. However, VTM relies on a different method, such as a lifting line model in Ref. [14], to provide blade aerodynamic (and by extension, aeroelastic) information necessary to formulate the initial vortex wake. Therefore, VTM solvers, such as VorTran-M [17] can be coupled with RANS CFD to provide accurate simulations of complex systems, such as wind turbines..

Results

Objectives

The Phase I proof-of-concept effort has built upon prior research efforts, presented in the prior section, to develop a hybrid computational aerodynamics code using a well-established massively parallel unstructured CFD method (FUN3D) to model the flow in near-body domains enclosing the wind turbine blades, nacelle and support structure encapsulated within a larger overset domain in which a vorticity-velocity formulation (VorTran-M) is used to predict the unsteady nature of the wake.

Prior developmental efforts focused on the rudimentary integration of the FUN3D and VorTran-M solvers, which supported only simple single grid configurations on single processor computers. In this Phase I effort, Georgia Tech and CDI generalized the coupling to support multiple grids and parallel operation. The primary Phase I objectives were:

- Generalization of the FUN3D/VorTran-M coupling interface that supports parallel operation and improvement of interface boundary conditions
- Development of interface to support an arbitrary number of grids and moving surfaces. This also included interfacing with the actuating blade model at GIT
- Validation of the FUN3D/VorTran-M coupling for steady and unsteady fixed wing problems, bluff bodies and multiple-grid rotor systems

FUN3D/VorTran-M Partial Parallelization

During Phase I, the prototype FUN3D/VorTran-M hybrid coupling was updated to support the latest FUN3D subroutines and the coupled code was set up so that FUN3D runs in parallel across multiple processors, and VorTran-M, a serial code, runs on the each processor. In this approach, which mirrors that employed in the OVERFLOW/VorTran-M coupling of [58, 65], FUN3D is parallelized as normal, but a copy of VorTran-M is present on every computer node.

The advantage of this approach over VorTran-M residing solely on the master node, is that the evaluation of BC velocities is handled locally (for entire grids, or grid components of split grids) on a given node rather than requiring additional synchronization and communication overhead to send and receive information from the master node. Moreover, this implementation is directly compatible with future instances using a parallel version of VorTran-M since every partition of the code is effectively identical.

Interface with Actuating Blade Approach

In previous work, the ability to use an actuator disk in the hybrid FUN3D/VorTran-M method was evaluated for rapid scaling analysis. While this actuator disk provides good estimates of the time-averaged pressures within its wake, the character of the wake is not captured, nor is the time dependency. An alternative to that is an actuator blade, where the sources that apply the pressure differential due to the rotor blades are placed only on the surface of the rotating, and possibly flapping/lagging and deforming, turbine blades rather than on the entire rotor disk (see, for example, Figure 6left). Including blade motion increases the cost significantly over the disk model since the source-grid node pairing must be searched, but in a parallel effort funded by NSF, this pairing algorithm was optimized using improved nearest neighbor searches [22]. The cost of this simulation has dropped by over two orders of magnitude depending on the number of processors used to resolve the actuating blades. This cost reduction, makes this source-actuation configuration a candidate for future turbine sizing design work

where prior to this an actuator disk would have been used. Indeed, such an approach can even form the basis of an interface to a structural dynamics code, where the loading can be fed between the two solvers at the source locations (this is in essence what happens in the original VTM rotorcraft analysis where an interpolation surface, rather than a formal actuating blade, is used near to insert the wake vorticity trailed and shed from turbine blades). The ability of the actuating blades to mimic the full unsteady wake is illustrated in Figure 6 (right) for a wind turbine rotor.

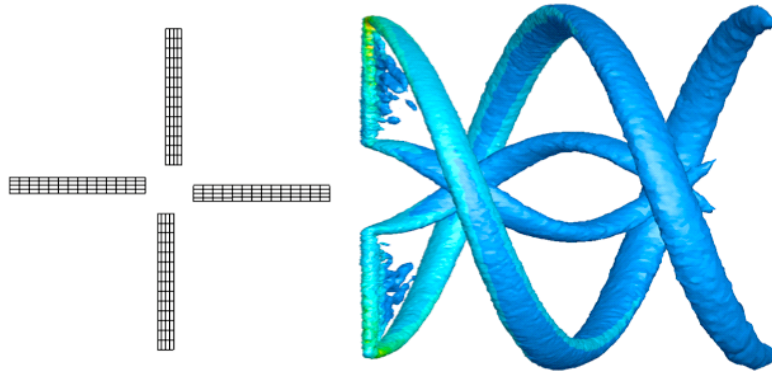


Figure 6: Actuating blades schematic; sources are located at the planform grid intersections and rotate with the blades (left). Incompressible wake simulation of an NREL rotor in 15m/s wind using an actuating blade with FUN3D (right)

Recent efforts have focused on developing the interface code to properly pass information between rotating and stationary reference frames, and an additional capability has been added to simulate an isolated (i.e. no tower) wind turbine, or rotor in axial flight, using only one blade in FUN3D to minimize computation time. Vorticity generated from the single blade is duplicated to the other blade locations during the vorticity insertion step. The full multi-bladed farfield wake influence and blade interactions are captured by VorTran-M. A proof-of-concept test of this approach is shown in Figure 7 for a 4 bladed hovering rotor (NACA0012 section and aspect ratio of 8.8). The hover flow condition was chosen since it is particularly difficult for traditional methods to predict and thus highlights the ability the coupled FUN3D/VorTran-M's ability to predict tip vortex evolution and blade vortex interactions. For example, in Figure 7c the tip vortex from the preceding blade interacts with the blade just inboard of the tip and two discrete vortices are observed to trail from the blade.

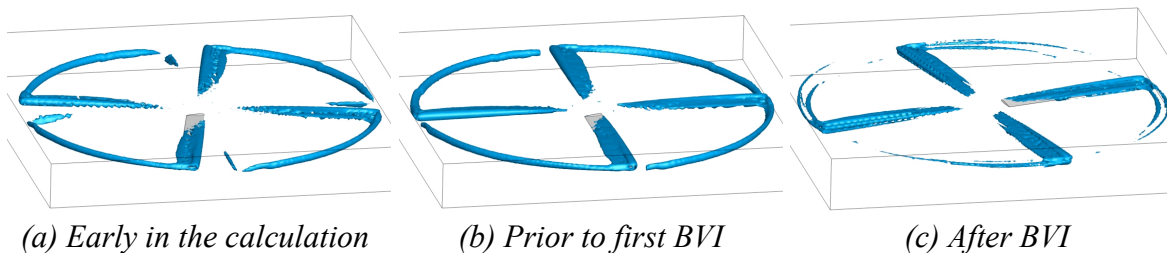


Figure 7: Simple four-bladed rotor in hover

Demonstration Cases

A critical component of the Phase I effort was to validate the FUN3D/VorTran-M methodology, through comparison with experimental data (where available, or known numerical results) for problems of relevance to the wind turbine community. Cases that were evaluated

include steady and unsteady wings, a circular cylinder in a cross-flow and a two-bladed hovering rotor.

Steady Fixed Wing

A finite fixed-wing configuration (rectangular wing, with aspect ratio of 8.8 using the NACA 0012 airfoil section) that has been previously applied to evaluate hybrid formulations of VorTran-M was also applied here [16,17]. Using a Mach number of 0.2 and the incompressible path within FUN3D, the wing was simulated at 5° angle of attack. A 240K node tetrahedral mesh that extended one chord length beyond the wing in all directions was used for these simulations.

To provide data for correlation, two-dimensional lift curve slopes (a_{2D}) from Abbott and von Doenhoff (6.3025/rad) were corrected for aspect ratio. These data were modified to account for three-dimensional effects using the well-known incompressible correction [67]:

$$a_{3D} = \frac{a_{2D}}{1 + \frac{a_{2D}}{\pi e_1 AR}} \quad (1)$$

The span effectiveness factor, e_1 , accounts for planform shape and wing taper as a function of aspect ratio. It varies from 0.95 to 1.0 for the 5° simulation, which corresponds to lift coefficients in the range of 0.44 to 0.45. For the FUN3D/VorTranM simulation, a lift coefficient asymptote of 0.47 is predicted. This is approximately a 5% over prediction of the theoretical data, but is in line with prior CFD/VorTran-M predictions with comparable size grids. These prior simulations have shown that increasing the near-body CFD grid extents using a 1.1 grid stretching factor, particularly in the wake (from 3c – 10c), improve the predictions to well within 1-2% of theory [16, 17]. This grid dependency will be further explored during the Phase II. The predicted drag is approximately 0.024, while estimates using Abbott and von Doenhoff [24] with induced drag estimates are about 0.02.

The same wing was run with varying grid resolutions at 8° angle of attack and, like prior fixed wing calculations showed the convection and preservation of the transient starting vortex for the entire duration of the simulation. Comparison of lift values with experimental data [24] and using Prandtl lifting-line aspect ratio corrections showed good agreement (Table 1). Most interestingly, a notable improvement in the predicted lift was observed over the baseline FUN3D, using an order of magnitude less cells!

Table 1: FUN3D predicted lift for NACA0012 wing at 8° angle of attack, compared with experimental data from [24]

Background grid	Fully coupled w/ VorTran-M	Total # of Cells	C_L	Error (%)
none	no	270k	0.7732	7.9
farfield → 5c	no	4.4M	0.7616	6.3
none	yes	420k	0.7326	2.2
-	-	-	0.7166	0.0

Unsteady Fixed Wing

To evaluate the behavior of the FUN3D/VorTran-M interface and boundary conditions with moving grids, an oscillating wing case, based upon the steady case presented above was investigated. In this configuration, there is asymmetric vortex shedding, and the flow field becomes more complex as the vortical structures interact with one another and convect downstream. The Mach number was 0.2 and the Reynolds number 4.5M for 5° pitch oscillations about a mean of 8° angle of attack with a reduced frequency $k=0.5$.

A sample wake for the oscillating wing is shown in Figure 8, and comparisons of the oscillating wing wake with the near-body FUN3D grid alone, a FUN3D overset simulation and a FUN3D/VorTran-M simulation are shown in Figure 9. The FUN3D near-body-alone simulation (top plot) shows that the shed vorticity is rapidly dissipated, while the full overset FUN3D simulation (bottom plot) shows less dissipation of the vorticity, illustrating the role of the longer wake and background grid in maintaining the integrity of the unsteady simulation. The magnitude of the local shed vorticity is maintained, but beyond one chord downstream dissipates quickly. The middle two figures illustrate the role of the VorTran-M cell size in maintaining to compactness of vortical structures. The upper middle figure has a cell size based on the FUN3D near-body grid average cell size. While fewer cells are needed using this algorithm to set the VorTran-M cell size, the strength of the shed vorticity is maintained, and further reduction of the VorTran-M cell size to 5% of the airfoil chord results in further improvement.

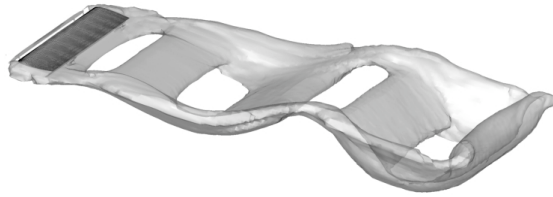


Figure 8: Iso-surfaces of vorticity magnitude for pitching NACA0012 wing predicted with FUN3D/VorTran-M

FUN3D/VorTran-M predictions of the unsteady lift and moment coefficients are compared to those from the high-resolution overset FUN3D case in Figure 10. The moment shows excellent correlation during the up and down strokes, matching both magnitude and phase, while the lift shows a slight reduction in magnitude due to the increased wake influence. The maximum and minimum values show some differences, less than 10% and 20% for the lift and moment respectively. The corresponding flow field evolution is shown in Figure 11 via vorticity magnitude. The figures demonstrate the preservation of the vortical structures downstream of the FUN3D near-body grid by VorTran-M.

Circular Cylinder in a Cross-Flow

The classical problem of a circular cylinder in a cross-flow is evaluated both in terms of predicted drag (and Strouhal number), but also in terms of the wake structure. A free-stream Mach number of 0.2 with a Reynolds number of 3900, similar to wind turbine towers was investigated. Predictions of the loading and the wake are shown in Figure 12 for a semi-infinite (periodic) FUN3D calculation, coupled with a (non-periodic) VorTran-M grid. Initially, both methods are comparable, but after a certain number of time steps, the wake in the VorTran-M method can no longer expand as needed, and differences arise. However, until that point, the simulation indicates that periodic computations are possible, given future modification of the VorTran-M boundary conditions to permit periodicity.

A finite cylinder (aspect ratio of 8.8) computation for the same flight conditions was next examined. The fully tetrahedral grid (Figure 13) consisted of 3M points, which is larger than the prior grids, and which acts also to demonstrate the capability of the parallel hybrid computations. It should be noted that Lynch [22] found that the tetrahedral grid was not the best for this problem; a mixed-element mesh with specified boundary layer aspect ratio cell sizes and growth were required to capture the most accurate surface characteristics. The FUN3D-alone grid spanned 19.5 diameters downstream, while the near-body FUN3D/VorTran-M grid spanned 3.5 diameters in the wake. Significant, aperiodic flows are observed, as was expected from the

configuration (Figure 14). The predicted primary Strouhal number for the FUN3D/VorTran-M simulation was computed as 0.2004, matching the FUN3D simulation [22].

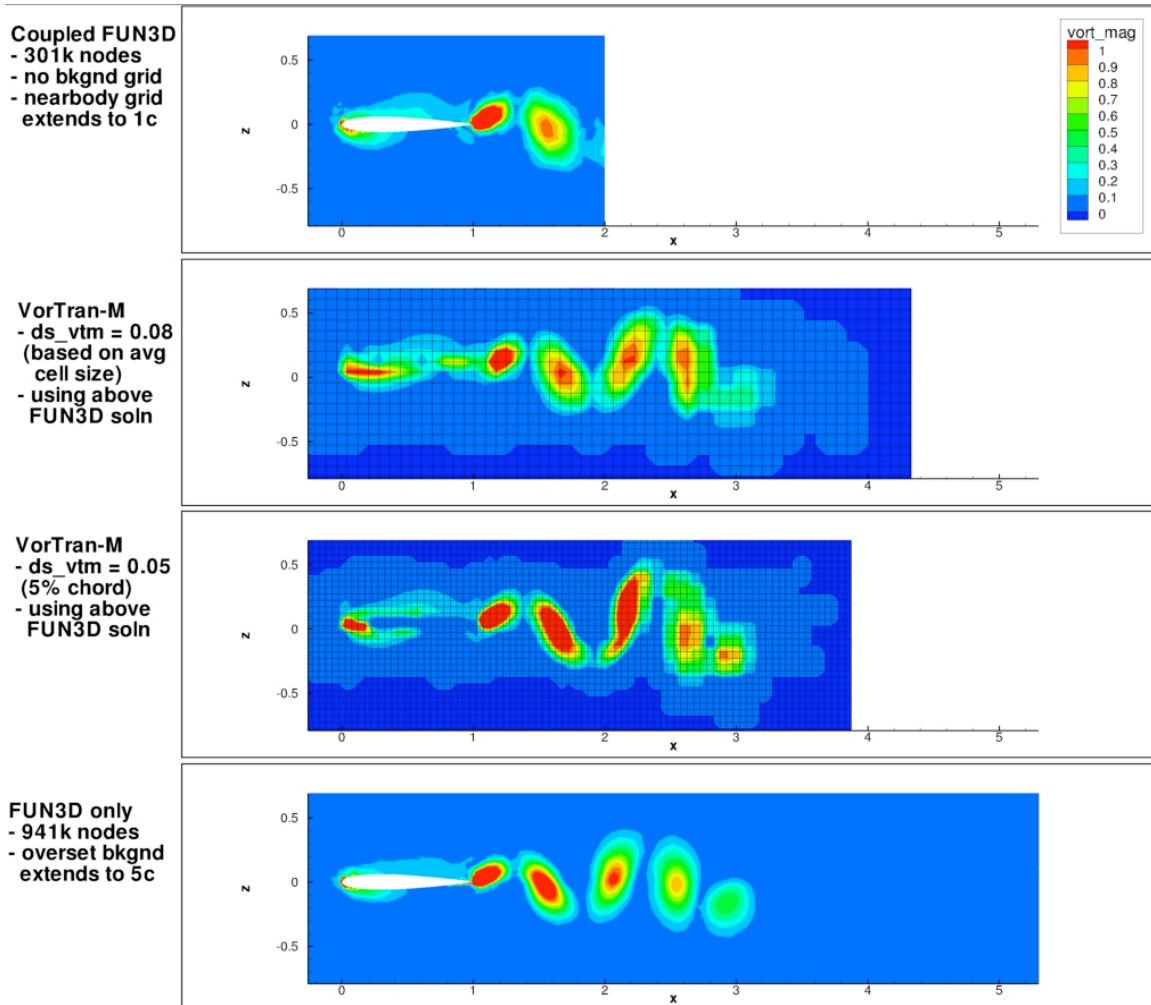


Figure 9: Comparisons of vorticity magnitude for an oscillating wing simulated with FUN3D and FUN3D/VorTran-M

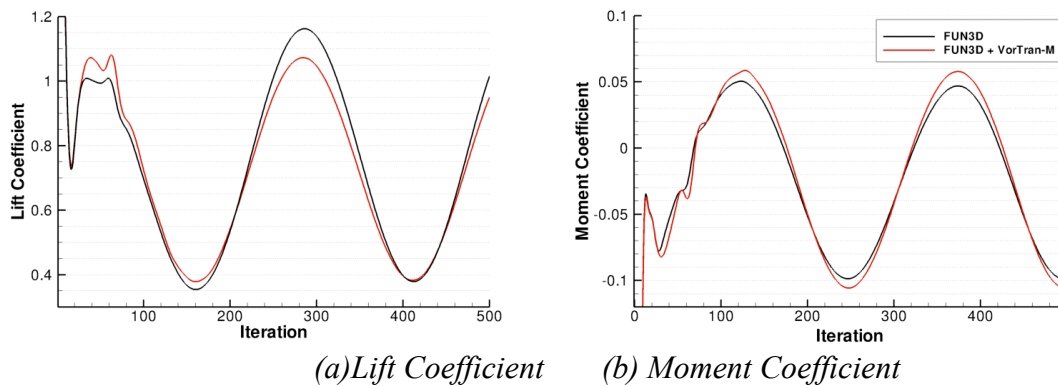


Figure 10: Comparisons of lift (left) and (right) moment coefficients for an oscillating wing

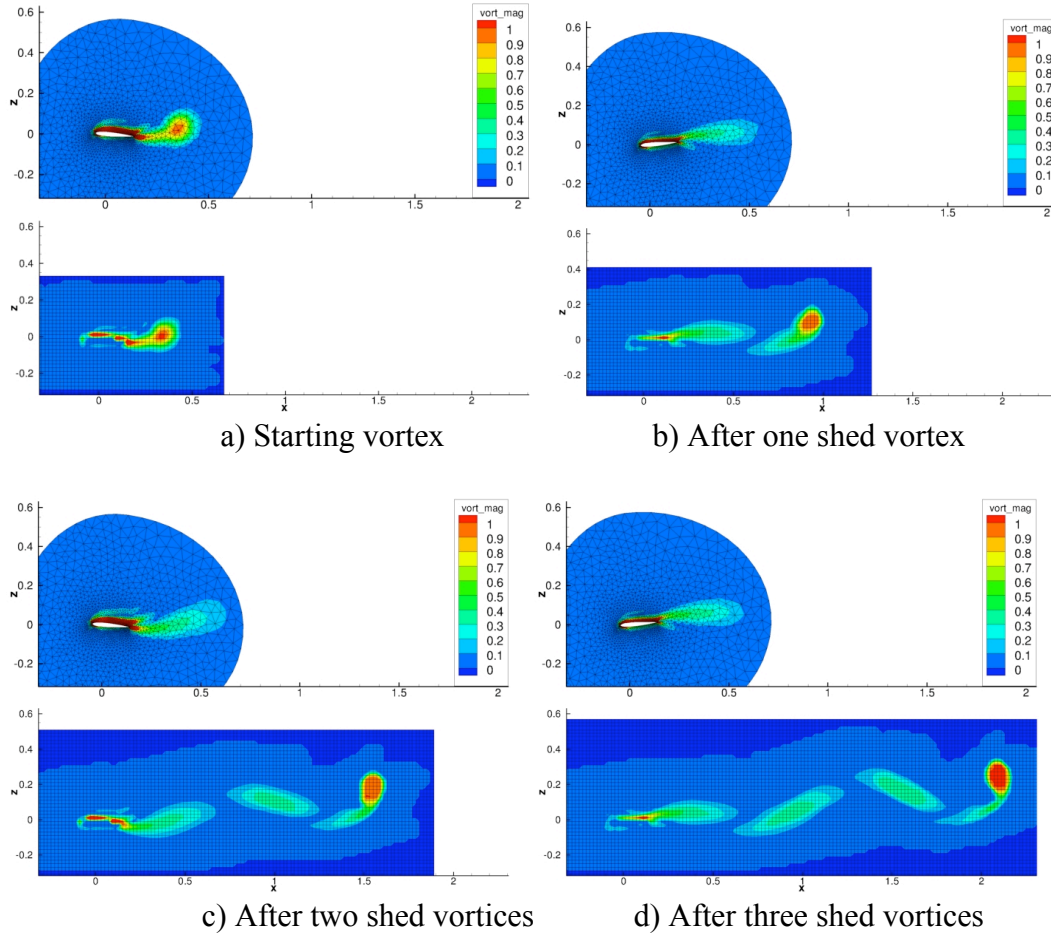


Figure 11: Time evolution of shed vorticity from FUN3D (top) and FUN3D/VorTran-M (bottom) for the oscillating airfoil.

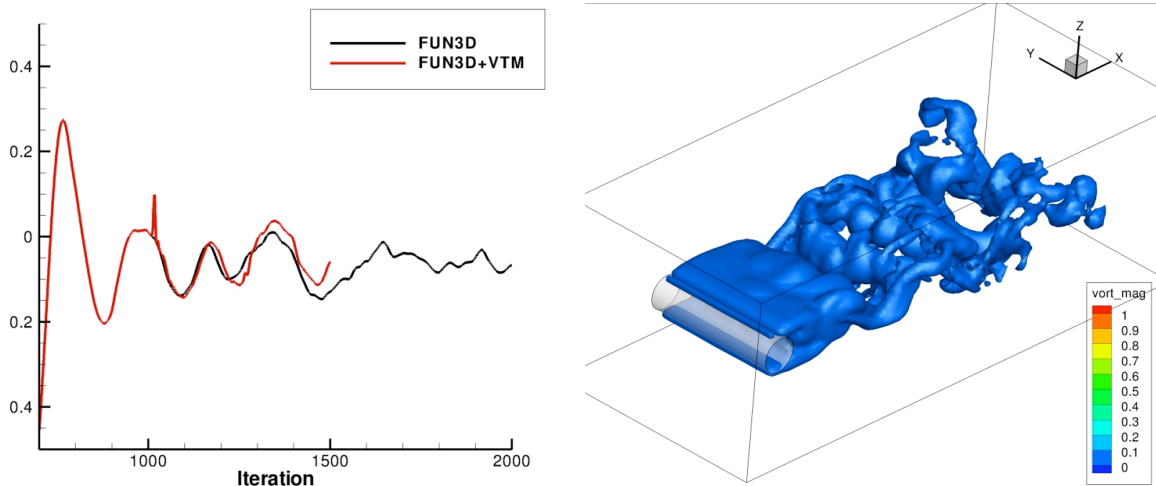
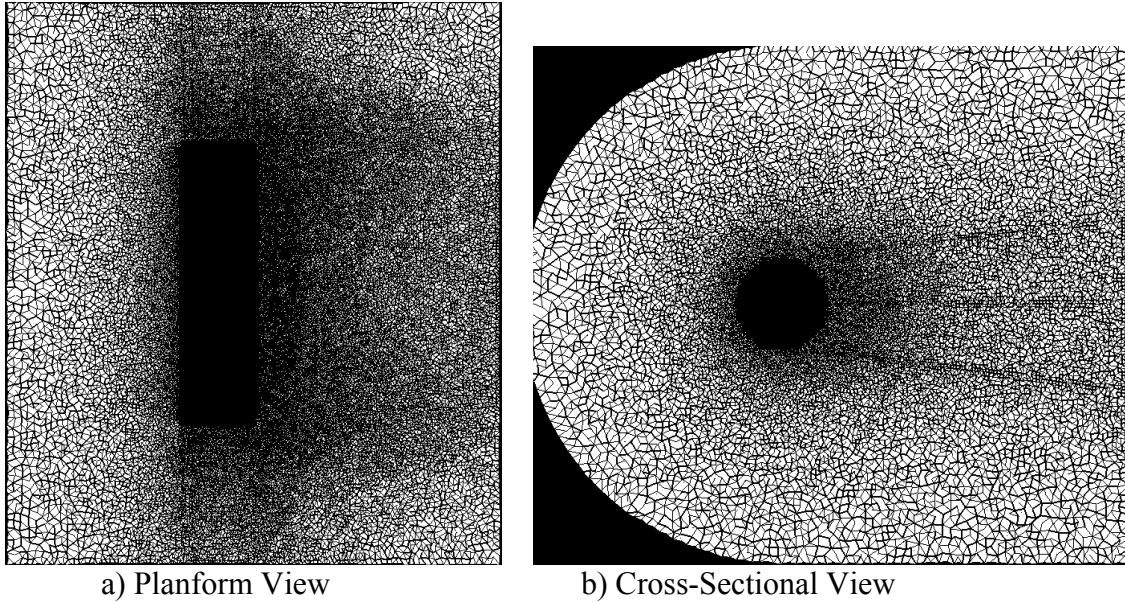


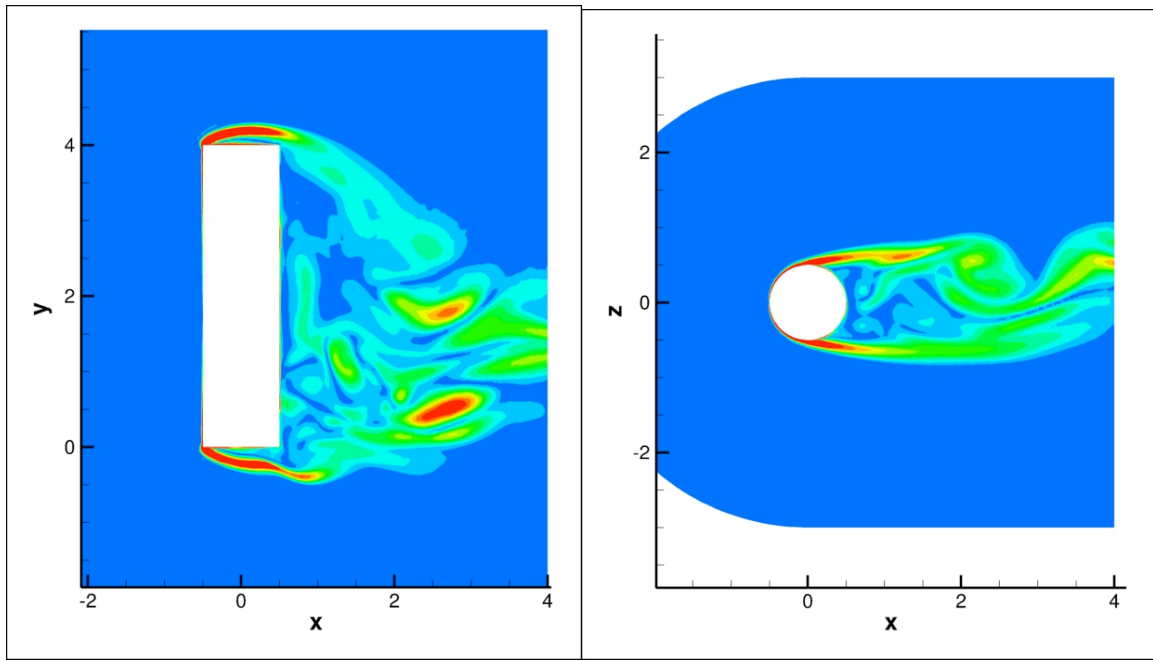
Figure 12: FUN3D and FUN3D/VorTran-M predictions of the drag on a circular cylinder (left) and the FUN3D/VorTran-M predicted wake structure (right)



a) Planform View

b) Cross-Sectional View

Figure 13: Views of Near-Body CFD tetrahedral grids for the finite cylinder.



a) Planform View of Vorticity

c) Cross-Plane View of Vorticity

Figure 14: Vorticity shed from FUN3D/VorTran-M simulation of finite cylinder in a cross-flow. ($M=0.2$, $Re=3900$)

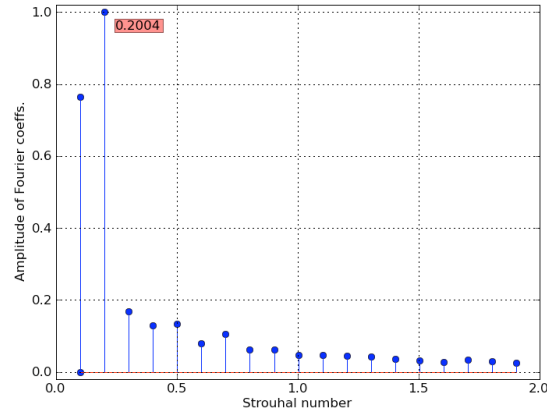


Figure 15: Strouhal number prediction for FUN3D/VorTran-M for the finite cylinder.

Two-Bladed Rotor at Zero Yaw

The two-bladed hovering rotor of Caradonna and Tung [20, 26] provides an excellent correlation case with which to evaluate the FUN3D/VorTran-M methodology. The rotor was simulated via an overset grid arrangement where only a single blade was modeled in FUN3D directly. Given the symmetry in the loading of the hover scenarios, the predicted flow field that initializes the VorTran-M vorticity distribution, can be duplicated, rotated by 180 degrees and inserted as a second blade as illustrated in Figure 16. The advantage of this approach is that the cost of the calculation can be reduced through the reduction of mesh nodes (as only one blade is modeled), while still retaining the full unsteady influence of two blades on the rotor wake.

A series of snapshots of the rotor wake illustrates in Figure 17 the capture of the blade-vortex interaction that is present, and demonstrates the build-up of the wake structure as VorTran-M captures the long-age wake in hover. The characteristic of the resulting flow field can be observed via vorticity in Figure 18.

For Phase II, the NREL wind turbine, whose grid is shown in Figure 19, will extend the demonstration of the methodology, including CSD and acoustics predictions.

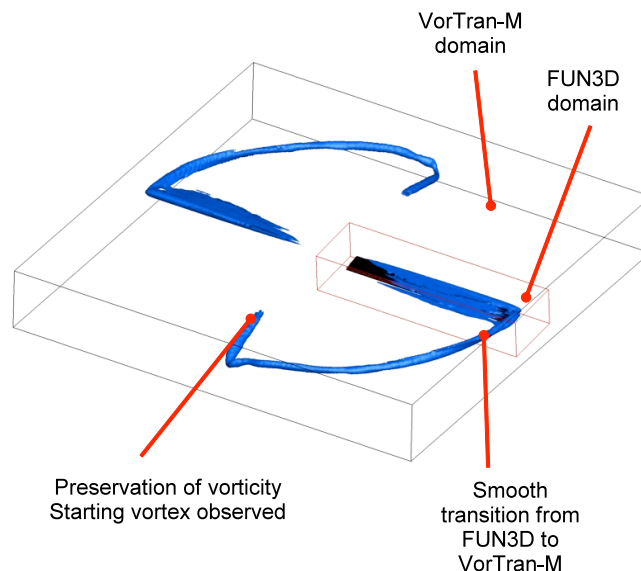


Figure 16: Schematic of FUN3D/VorTran-M grid arrangement for the two bladed rotor in hover

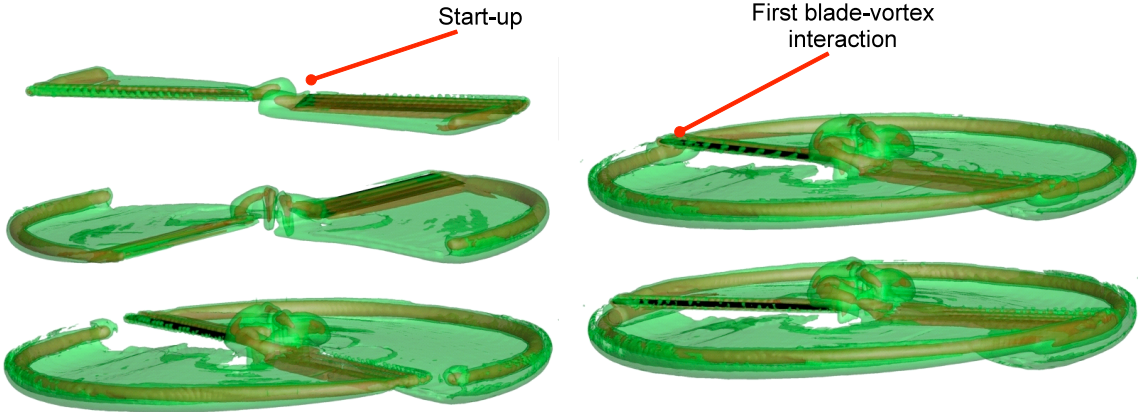
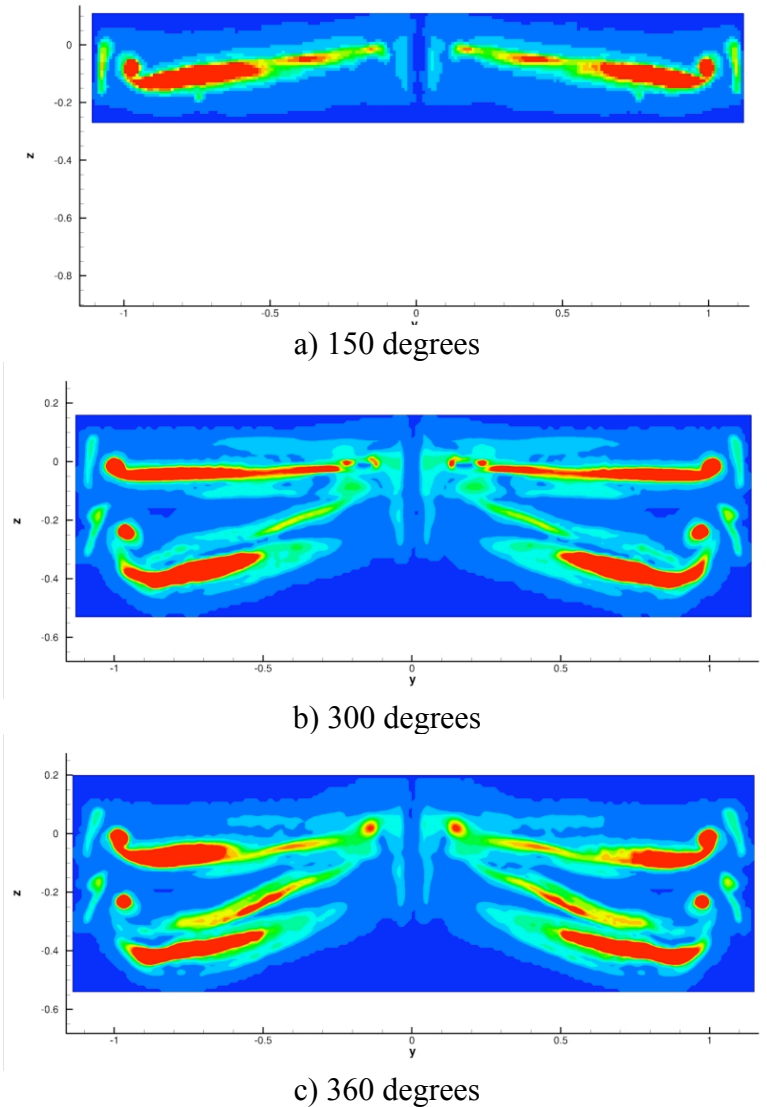
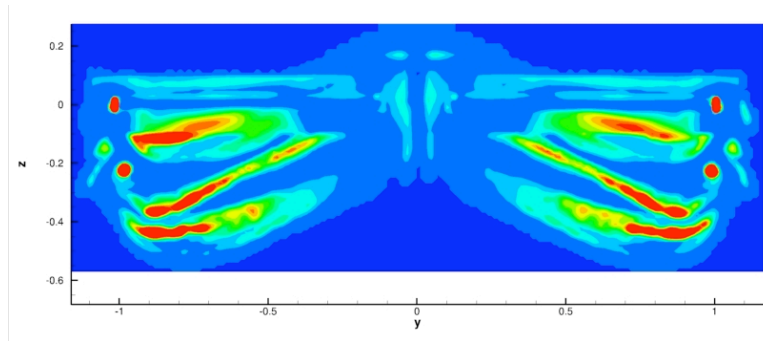


Figure 17: Snapshots of the hovering rotor wake predicted by FUN3D/VorTran-M





d) 450 degrees

Figure 18: Illustration of the temporally developing wake of a hovering rotor (wind turbine at zero yaw) captured by FUN3D/VorTran-M. The vorticity magnitude illustrates the crispness of the vortex sheet and tip vortex as it moves away from the rotor blade.

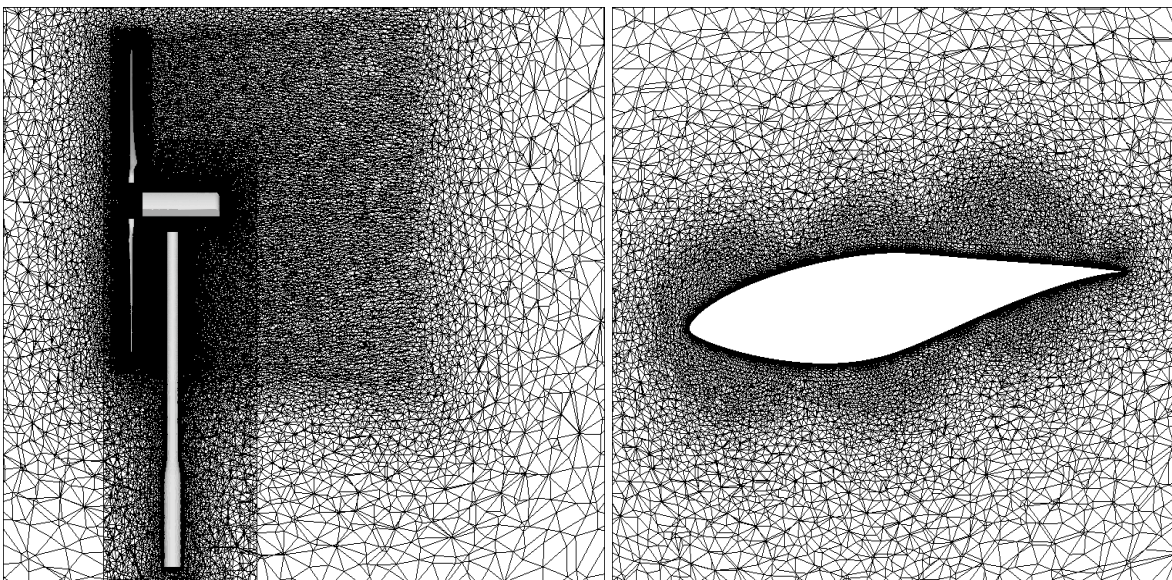


Figure 19: Unstructured grid for the NREL Phase VI HAWT configuration. 2.6 million nodes per blade, 7.2 million nodes total.

References

1. Linowes, L., "Catastrophic Turbine Failure at Vermont Wind Farm Raises Doubt About Turbine Safety, Longevity ". 2008, Industrial Wind Action Group, <http://www.windaction.org/releases/18394>.
2. Anon., "India's Suzlon Finishes Retrofit of Wind Blades." 2009, Reuters, <http://www.reuters.com/article/ELECTU/idUSN1254602620091012>; Los Angeles, CA.
3. Wright, T., "Suzlon's US Wind Turbine Plans Hit New Turbulence," *Wall Street Journal*. 2008, <http://www.livemint.com/2008/07/01003655/Suzlon8217s-US-wind-turbine.html>; New York, NY.
4. Whitehouse, G.R., A.H. Boschitsch, T.R. Quackenbush, D.A. Wachspress, and R.E. Brown. "Novel Eulerian Vorticity Transport Wake Module for Rotorcraft Flow Analysis." *8th Symposium on Overset Composite Grids & Solution Technology*. 2006. Houston, TX.
5. Anon., "FUN3D-Analysis and Design." 2007, NASA <http://fun3d.larc.nasa.gov>

6. O'Brien, D.M. and M.J. Smith. "*Improvements in the Computational Modeling of Rotor/Fuselage Interactions Using Unstructured Grids.*" *61st Annual Forum of the American Helicopter Society.* 2005. Grapevine, TX.
7. Renaud, T., D. O'Brien, M.J. Smith, and M. Potsdam, "*Evaluation of Isolated Fuselage and Rotor-Fuselage Interaction Using CFD.*" *Journal of the American Helicopter Society,* 2008. Vol. 52(No. 1).
8. Lynch, C.E. and M.J. Smith. "*Hybrid RANS-LES Turbulence Models on Unstructured Grids*" *38th AIAA Fluid Dynamics Conference and Exhibit.* 2008. Seattle, WA: AIAA-2008-3854
9. Abras, J.N. and M.J. Smith. "*Rotorcraft Methodology For Unstructured CFD-CSD Coupling.*" *AHS Aeromechanics Specialist's Conference.* 2008. San Francisco, CA.
10. Thepvongs, S., J.R. Cook, C.E.S. Cesnick, and M.J. Smith. "*Computational Aeroelasticity of Rotating Wings with Deformable Airfoils.*" *65th Annual Forum of the American Helicopter Society.* 2009. Grapevine, TX.
11. Nielsen, E.J. "*Aerodynamic Design Optimization Using the Navier-Stokes Equations.*" *18th International Symposium on Mathematical Programming.* 2003. Copenhagen, Denmark.
12. Abras, J.N., C.E. Lynch, and M.J. Smith. "*Advances in Rotorcraft Simulations with Unstructured CFD.*" *63rd Annual Forum of the American Helicopter Society.* 2007. Virginia Beach, VA,.
13. Biedron, R.T. and E.M. Lee-Rausch. "*Rotor Airloads Prediction Using Unstructured Meshes and Loose CFD/CSD Coupling.*" *26th AIAA Applied Aerodynamics Conference.* 2008. Honolulu, HI: AIAA-2008-7341.
14. Fletcher, T.M. and R.E. Brown. "*Simulating Wind Turbine Interactions using the Vorticity Transport Equations*" *8th ASME Wind Energy Symposium.* 2009. Orlando, FL.
15. Komerath, N., Smith, M.J., and Tung, C., "
16. Whitehouse, G.R., A.H. Boschitsch, T.R. Quackenbush, D.A. Wachspress, and R.E. Brown, "*Novel Eulerian Vorticity Transport Wake Model for Rotorcraft Flow Analysis.*" 2009, Continuum Dynamics, Inc. CDI Report No. 09-02 & RDECOM TR 08-D-73.
17. Whitehouse, G.R., A.H. Boschitsch, T.R. Quackenbush, D.A. Wachspress, and R.E. Brown. "*Novel Eulerian Vorticity Transport Wake Module for Rotorcraft Flow Analysis.*" *63rd Annual Forum of the American Helicopter Society.* 2007. Virginia Beach, VA.
18. Whitehouse, G.R. and H. Tadghighi, "*Investigation of Hybrid Grid-Based CFD Methods for Rotorcraft Flow Analysis.*" *Journal of the American Helicopter Society,* 2011.
19. Whitehouse, G.R. and H. Tadghighi. "*Investigation of Hybrid Grid-Based CFD Methods for Rotorcraft Flow Analysis.*" *AHS Specialist's Conference on Aeromechanics.* 2010. San Francisco, CA.
20. Caradonna, F.X. and C. Tung, "*Experimental and Analytical Studies of a Model Helicopter Rotor in Hover.*" 1981, NASA-TM-81232, USAAVRADCOM TR-81-A-23.
21. Whitehouse, G.R., A.H. Boschitsch, M.J. Smith, C.E. Lynch, and R.E. Brown. "*Investigation of Mixed Element Hybrid Grid-Based CFD Methods for Rotorcraft Flow Analysis.*" *66th Annual Forum of the American Helicopter Society.* 2010. Phoenix, AZ.
22. Lynch, C.E., "*Advanced CFD Methods for Wind Turbine Analysis,*" *PhD Thesis, Aerospace Engineering.* 2011, Georgia Institute of Technology: Atlanta, GA.
23. Anderson, J.D., Jr., *Aircraft Performance and Design.* 1999: WCB McGraw-Hill.
24. Abbott, I.H. and A.E. VonDoenhoff, *Theory of Wing Sections.* First ed. 1959, New York: Dover Publications.

25. O'Brien, D.M., "*Analysis Of Computational Modeling Techniques For Complete Rotorcraft Configurations*," *School of Aerospace Engineering*. 2006, Georgia Institute of Technology, PhD.
26. Caradonna, F.X. and C. Tung, "*Experimental and Analytical Studies of a Model Helicopter Rotor in Hover*." *Vertica*, 1981. **Vol. 5**: p. pp. 149-161.
27. Stone, C., M. Barone, M.J. Smith, and E. Lynch. "*A Computational Study of the Aerodynamics and Aeroacoustics of a Flatback Airfoil Using Hybrid RANS-LES* " *47th AIAA Aerospace Sciences Meeting including The New Horizons Forum and Aerospace Exposition*. 2009. Orlando, FL: AIAA-2009-273.
28. Stone, C., E. Lynch, and M.J. Smith. "*Hybrid RANS/LES Simulation of the NASA/NREL Phase- VI Horizontal Axis Wind Turbine* " *48th AIAA Aerospace Sciences Meeting including The New Horizons Forum and Aerospace Exposition*. 2010. Orlando, FL: AIAA-2010-0459.